Title

Transcriptomic Analysis of Right Ventricular Remodeling in Two Rat Models of Pulmonary Hypertension: Identification and Validation of Epithelial-to-Mesenchymal Transition in Human Right Ventricular Failure.

Journal

Circulation. Heart failure, 14(2)

ISSN

1941-3289

Authors

Park, John F
Clark, Varina R
Banerjee, Somanshu
et al.

Publication Date

2021-02-01

DOI

10.1161/circheartfailure.120.007058

Peer reviewed

HHS Public Access

Author manuscript

Circ Heart Fail. Author manuscript; available in PMC 2022 February 05.

Published in final edited form as:

Circ Heart Fail. 2021 February ; 14(2): e007058. doi:10.1161/CIRCHEARTFAILURE.120.007058.

Transcriptomic Analysis of Right Ventricular Remodeling in Two Rat models of Pulmonary Hypertension: Identification and Validation of EMT in Human Right Ventricular Failure

John F Park, M.D., Ph.D[1], **Varina R Clark, B.Sc**[1,*], **Somanshu Banerjee, PhD**[1,*], **Jason Hong, M.D.**[1,3], **Asif Razee, M.Sc**[1], **Tiffany Williams, M.D., Ph.D**[1], **Gregory Fishbein, M.D.**[2], **Lou Saddic, M.D., Ph.D**[1], **Soban Umar, M.D., Ph.D**[1]

[1]Department of Anesthesiology and Perioperative medicine, Division of Molecular Medicine, David Geffen School of Medicine, UCLA, Los Angeles, CA

[2]Department of Pathology, David Geffen School of Medicine, UCLA, Los Angeles, CA

[3]Department of Medicine, Division of Pulmonary Critical Care Medicine, UCLA, Los Angeles, CA

Abstract

Background: Right ventricular (RV) dysfunction is a significant prognostic determinant of morbidity and mortality in pulmonary arterial hypertension (PAH). Despite the importance of RV function in PAH, the underlying molecular mechanisms of RV dysfunction secondary to PAH remain unclear. We aim to identify and compare molecular determinants of RV failure using RNA-sequencing of RV tissue from two clinically relevant animal models of PAH.

Methods: We performed RNA-sequencing on RV from rats treated with monocrotaline (MCT) or Sugen with hypoxia/normoxia (SuHx). PAH and RV failure were confirmed by catheterization and echocardiography. We validated the RV transcriptome results using quantitative real-time PCR, immunofluorescence and Western blot. Immunohistochemistry and immunofluorescence were performed on human RV tissue from control (n=3) and PAH-induced RV failure patients (n=5).

Results: We identified similar transcriptomic profiles of RV from MCT- and SuHx-induced RV-failure. Pathway analysis showed genes enriched in epithelial-to-mesenchymal transition (EMT), inflammation, and metabolism. Histological staining of human RV tissue from patients with RV-

Correspondence: Soban Umar, M.D., Ph.D, Assistant Professor-in-Residence, Department of Anesthesiology and Perioperative Medicine, Division of Molecular Medicine, UCLA Cardiovascular Theme, David Geffen School of Medicine at UCLA, 650 Charles E Young Drive South BH557 CHS, Los Angeles, CA 90095, USA, sumar@mednet.ucla.edu, Phone: 310-794-7804.

*Contributed equally and to be considered co-2nd authors

Author Contributions:

John F Park, M.D., Ph.D: Contributed to overall design of study, and acquisition, analysis, and interpretation of data. Drafted and revised manuscript for intellectual content. Approved final version of manuscript for publication.

Varina Clark, B.Sc: Contributed to acquisition and analysis of data. Revised manuscript for intellectual content.

Somanshu Banerjee, Ph.D: Contributed to acquisition and analysis of data. Revised manuscript for intellectual content.

Jason Hong, M.D. : Contributed to acquisition and analysis of data. Revised manuscript for intellectual content.

Asif Razee, M.Sc: Contributed to acquisition and analysis of data. Revised manuscript for intellectual content.

Tiffany Williams, M.D., Ph.D: Contributed to acquisition and analysis of data.

Gregoire Fishbein, M.D.: Provided human samples for study.

Lou Saddic, M.D., Ph.D: Contributed to acquisition and analysis of data.

Soban Umar, M.D., Ph.D: Contributed to overall design of study, and acquisition, analysis, and interpretation of data. Revised manuscript for intellectual content. Approved final version of manuscript for publication.

Disclosure Statement: None

failure secondary to PAH revealed significant RV fibrosis and endothelial-to-mesenchymal transition (EndMT), as well as elevated CCN2 (top gene implicated in EMT/EndMT) expression in perivascular areas compared to normal RV.

Conclusions: Transcriptomic signature of RV failure in MCT and SuHx models showed similar gene expressions and biological pathways. We provide translational relevance of this transcriptomic signature using RV from PAH patients to demonstrate evidence of EMT/EndMT and protein expression of CCN2 (CTGF). Targeting specific molecular mechanisms responsible for RV failure in MCT and SuHx models may identify novel therapeutic strategies for PAH-associated RV failure.

List of Key Words:

PAH; Right Ventricular Failure; Transcriptomics; EndMT; CTGF

Introduction

Pulmonary arterial hypertension (PAH) is a progressive, fatal disease characterized by pathological arterial remodeling leading to increased pulmonary vascular resistance (PVR), right ventricular (RV) hypertrophy, RV failure, and death.[1,2] Although current therapies targeting pulmonary vasculature have resulted in some functional improvement for patients with PAH-induced RV failure, survival remains poor.[1,2] Previous studies have demonstrated that symptom severity and survival in PAH are closely linked to RV remodeling and function.[2] RV remodeling due to chronic pressure overload causes a number of adaptations in size, shape, and structure, and can lead to significant RV dysfunction.[3] It is a complex process that leads to cardiomyocyte hypertrophy, fibrosis, inflammation, angiogenesis, and metabolic changes. In PAH patient, the adaptation of the RV to high pulmonary arterial pressures is the most important determinant of prognosis. However, the underlying molecular mechanism of adverse RV remodeling and dysfunction is poorly understood, and there are no currently approved therapies that improve RV function.[1]

Recent evidence suggests RV fibrosis to play a crucial role in the development of RV failure. Increased fibrotic deposition, characterized by myofibroblast accumulation and excessive collagen secretion, can result in RV stiffness and severe dysfunction.[4] Recent studies have implicated epithelial-to-mesenchymal transition (EMT) and endothelial-to-mesenchymal transition (EndMT) to play a role in adult cardiovascular disease and fibrosis. In response to cardiac injury, a significant portion of myofibroblasts arise from the conversion of epithelial or endothelial cells through the EMT or EndMT process, respectively, and ultimately lead to excessive collagen deposition, fibrosis and cardiac dysfunction.[5,6] EndMT has been shown to play a critical role in myocardial fibrosis and diastolic dysfunction in pressure-overload rodent models.[6,7]

Monocrotaline (MCT) toxin and vascular endothelial growth factor (VEGF) receptor antagonist (SU5416) combined with chronic hypoxia followed by normoxia (SuHx) represent two important animal models that induce PAH and RV failure in response to pressure overload.[8] Most studies in RV remodeling due to PAH have used MCT model, but off-target effects of MCT have greatly limited its clinical relevance.[1] SuHx model is

considered an important pre-clinical model of PAH due to its occlusive plexiform-like lesions in the lung, which closely resemble human PAH.[9] This model also leads to severe RV dysfunction with marked hypertrophy, which are important features of RV failure due to PAH. Here, we performed comparative transcriptomic analysis of RV failure in MCT and SuHx PAH models using RNA sequencing. This study provides a comprehensive understanding of dysregulated genes and pathways involved in PAH rats with RV failure, and further validation of transcriptomic signature in human RV failure patients with PAH.

Materials and Methods

The data that support the findings of this study are available from the corresponding author upon reasonable request.

Development of RV failure in PAH rats

All animal studies were performed in accordance with the National Institutes of Health (NIH) Guide for the Care and Use of Laboratory Animals. Adult male Sprague Dawley rats (250–350g) received either a single subcutaneous injection of endothelial toxin Monocrotaline (MCT, 60mg/kg, MCT group, n=7) and were followed for ~30 days or VEGF-receptor antagonist Sugen (SU5416, 20mg/kg, SuHx group, n=7) and kept in hypoxia (10% oxygen) for 3-weeks followed by 2-weeks of normoxia. Phosphate buffered saline (PBS) treated rats served as controls (CTRL group, n=7). Transthoracic echocardiography was performed to monitor cardiopulmonary hemodynamics using a Vevo 2100 high-resolution image system. The right ventricular systolic pressure (RVSP) was measured directly by a catheter connected to a pressure transducer (ADInstruments) into the RV.

RNA Sequencing and functional analysis

Libraries for RNA-seq were prepared using SMARTer Stranded Total RNA-Seq Kit v2 - Pico Input Mammalian (Takara Bio) and sequenced using Hiseq 3000 (Illumina). Differential expression analysis was performed using the DESeq2 R package version 1.25.16. DEGs with false discovery rate (FDR) <0.05 based on Benjamini Hochberg algorithm were considered statistically significant. Gene set enrichment analysis was performed using the Bioconductor (release 3.1) fgsea[10] and R (version 3.6.1) software package. Hallmark[11] and Reactome[12] gene sets were obtained from molecular signature database (MSigDB).[13] Enriched pathways considered statistically significant were defined by adjusted p-value <0.05.

RNA Extraction and quantitative real-time PCR

Total RNA was isolated from rat RV and LV tissue using Trizol (Invitrogen). Quantitative real-time PCR was performed with iTaq Universal SYBR (Bio-Rad). GADPH was used as an internal reference control, and relative gene expression was normalized to PBS-treated group.

Western Blot Analysis

Protein lysates were prepared from rat RV and LV tissue using modified RIPA lysis buffer containing protease and phosphatase inhibitor cocktails (Sigma). Proteins were diluted in 4x

Laemmli sample buffer, boiled, separated on 10% gels (Bio-Rad) by SDS page and subsequently transferred onto nitrocellulose membranes (Bio-Rad) using semi-dry blotting (TransBlot Turbo System, Bio-Rad). After transfer, membranes were blocked with 5% bovine serum albumin (Sigma) and incubated with antibodies directed against CTGF (Abcam #ab6992; 1:200) and Vinculin (Sigma #V9131; 1:5000). IR Dye-conjugated secondary antibodies (LI-COR) were used for detection and blots were scanned and quantified using the LI-COR Odyssey Infrared Imaging System and Image Studio Lite.

Histologic assessment and immunofluorescence staining

The RV wall, the left ventricular (LV) wall, and the interventricular septum (IVS) were dissected and weighed. The ratio of the RV to LV plus septal weight [RV/(LV + IVS)] was calculated as the Fulton index of RV hypertrophy. Rat heart OCT sections were stained with antibodies against anti-αSMA (Sigma #A2547; 1:400), anti-CD31 (Novus Biologicals #NB100–2284; 1:100), or anti-CTGF (CCN2, Abcam #ab6992; 1:500). Paraffin embedded human RV free wall sections were stained with Masson's trichrome staining according to manufacturer's protocol (Sigma) or with antibodies against anti-αSMA, anti-VWF, or anti-CTGF (CCN2). Percent RV tissue fibrosis was determined as previously described.[14] VWF and αSMA positive vessels were counted manually at 10x objective from at least 20 images across the RV section. Mean fluorescence intensity was calculated by at least 15 images across the RV sections and then analyzed with ImageJ software (http://rsb.info.nih.gov/ij/). Sections were imaged with Nikon confocal microscope.

Human RV Tissue acquisition and characteristics

We acquired human RV sections (RV free wall) from non-heart failure donor hearts (control group; n=3) and right heart failure patients with PAH (RV Failure; n=5) from the Department of Pathology at University of California, Los Angeles (UCLA). De-identified clinical dataset were obtained for each patient. Right heart dysfunction due to PAH was evaluated by right heart catheterization (Table E6).

Statistical Analysis

To assess differences between groups, Welch's Unpaired t-test and one-way ANOVA tests were used due to potential assumption violations (equal variance) using the more standard tests. When significant differences were detected, individual mean values were compared by post-hoc tests that allowed for multiple comparisons with adequate type I error control (Bonferroni). Analyses were run using GraphPad Prism and p-values<0.05 was considered statistically significant. Values are expressed as mean ± SD.

Results

Development of severe PAH and RV failure in MCT and SuHx rats

We first confirmed severe PAH and RV failure using serial non-invasive echocardiography and terminal right heart catheterization in rats treated with MCT or SuHx compared to PBS-treated rats for control (Figure 1A). Both MCT and SuHx rats showed significant PAH as evidenced by increased RVSP (MCT: 90.6±16.0, p<0.0001; SuHx: 90.8±18.7, p<0.0001), and decreased pulmonary artery acceleration time (PAT) (MCT: 21.1±6.2, p=0.1; SuHx:

18.5±.2.3, p=0.01) and PAT/pulmonary ejection time (PET) ratio (MCT: 0.3±0.1, p=0.04; SuHx: 0.2±0.0, p=0.001) compared to control (Figure 1C; Table 1). RV dysfunction was demonstrated by increased RV internal diameter at end-diastole ($RVID_d$) (MCT: 3.0 ± 0.9, p=0.0006; SuHx: 2.7 ± 0.8, p=0.0043) and decreased RV fractional area change (RVFAC) in MCT and SuHx rats (MCT: 18.6±10.8, p=0.0044; SuHx: 15.8±5.7, p=0.0014) compared to control (Figure 1B, C; Table 1). MCT and SuHx rats also demonstrated an increase in RV hypertrophy index (RV/LV+IVS) (MCT: 0.7±0.2, p<0.0001; SuHx: 0.6±0.2, p=0.0003). No significant differences were observed between SuHx- and MCT-treated groups.

Similar transcriptome signature of RV failure in MCT and SuHx rats

After confirmation of severe RV dysfunction, RNA sequencing of RV tissue from MCT (n=4) and SuHx (n=4) rats revealed 7,842 and 3,146 differentially expressed genes (DEG), respectively, compared to control rats (n=4) based on FDR <0.05 (Figure 2, 3A, Table E1 and E2). Hierarchical clustering of top DEGs (FDR <0.05) in the RV showed similar gene signatures between MCT and SuHx rats compared to control (Figure 2), with mild variability within the SuHx group. Both MCT- and SuHx-treated groups shared 2,693 DEGs in the RV that were either up- or down-regulated in a similar fashion (Figure 3A, 3C). The top 20 up- and down-regulated transcripts according to log2fold change and p-value threshold of <0.05 in RV of MCT and SuHx-treated groups are shown in Figure 3B. SPP1 and AHRR were the most up-regulated DEG in MCT and SuHx-treated group, respectively compared to control. Myo16 and Proz were the most down-regulated DEGs in MCT and SuHx-treated group, respectively compared to control.

Multiple pathways are commonly altered in RV of MCT- and SuHx-induced RV failure

We performed a ranked-based directional enrichment analysis of RV transcriptome from MCT and SuHx rats compared to control. Since previous studies reported RV failure being associated with RV fibrosis, inflammation, and angiogenesis in MCT- and SuHx-models[15,16], we used a refined collection of gene sets (Hallmark) that includes these biological processes.[11] We identified 32 and 30 Hallmark pathways significantly enriched in MCT and SuHx rats, respectively with 25 pathways overlapping (Figure 4A, Table E3). The top up-regulated enriched pathways in RV of MCT and SuHx rats according to FDR <0.05 were EMT and tumor-necrosis factor-alpha (TNF-α) signaling *via* nuclear factor-kB (NFkB). The top down-regulated enriched pathways in both MCT and SuHx rats were oxidative phosphorylation and fatty acid metabolism (Figure 4B). Inflammatory response and angiogenesis were also significantly enriched in both MCT- and SuHx-treated groups.

To further explore specific biological processes, we used Reactome pathway enrichment analysis[12] of RV from MCT and SuHx rats. Extracellular matrix organization and interleukin-10 signaling were the top up-regulated enriched pathways in MCT and SuHx rats, respectively. The citric acid TCA cycle and respiratory electron transport were the top down-regulated enriched pathways in MCT and SuHx rats (Table E4).

qPCR validation of selected genes from enrichment pathway analysis

To validate the RNA sequencing results and gene expression changes, we selected DEGs from significantly enriched pathways that were identified by Hallmark analysis for qRT-

PCR. PCR results of DEGs in the RV from EMT (SPP1, CCN2), TNF-α signaling *via* NFκB (IL7R), oxidative phosphorylation (ACAT1, COX7B), fatty acid metabolism (DECR1, HSP90A), inflammation (C5AR1) and angiogenesis (S100A4) were consistent with the RNA sequencing results (Figure 5A). In contrast, PCR results in the LV for SPP1, C5AR1, HSP90A, ACAT1, COX7B, and DECR1 showed no significant change in gene expression from SuHx and MCT rats compared to control. Though, we did observe significant up-regulation of S100A4 in SuHx ($p=0.007$) and MCT ($p=0.003$), CCN2 in SuHx ($p<0.001$), and IL7R in SuHx ($p=0.006$) compared to control (Figure 5B). No significant difference in gene expression levels between SuHx and MCT were noted.

Demonstration of EndMT/EMT in RV of MCT- and SuHx-induced RV failure

To evaluate the relevance of our RV transcriptome results in the context of RVF, we focused on EndMT/EMT, the top up-regulated enriched pathway in RV of MCT and SuHx rats. RV sections were stained with antibodies against α-SMA (myofibroblast marker) and CD31 (endothelial cell marker). Co-localization of α-SMA and CD31 is considered as evidence for EndMT (Figure 6).

To identify significant genes involved in EMT/EndMT, we created a list of genes based on Hallmark EMT gene set that were statistically significant (FDR <0.05) in both MCT and SuHx RV tissue (Table E5). Based on log2fold change, we identified SPP1 and CCN2 as the top up-regulated genes associated with EMT pathway. To validate their association with EMT and RV failure, we assessed CTGF (CCN2) immunolocalization in the RV which appears to be localized to vascular/perivascular areas and within the cardiomyocytes (Figure 7A). We also measured the expression of CTGF protein in MCT and SuHx rats using Western blot analysis. We found an increased RV expression of CTGF in SuHx ($p=0.0362$) and MCT rats ($p=0.0016$), whereas no significant differences were found in the LV (Figure 7B, C).

Validation of rat RV transcriptome in human right heart failure

To evaluate the clinical relevance of our RV transcriptome results in the context of RVF, we focused on EMT—the top up-regulated enriched pathway in RV of MCT and SuHx rats—in human RV sections from patients with RV failure secondary to PAH (n=5) and normal RV controls (n=3) (Table E6). Given the role of EMT and EndMT in cardiac fibrosis during chronic pressure overload[6,17], we first stained human RV tissues with Masson's trichome. Fibrosis in both interstitial and perivascular areas increased in RV of human PAH compared to control (RVF: 49.5±9.0, Ctrl: 19.9±2.6, $p=0.028$) (Figure 8A, B). Human RV sections were further stained with antibodies against α-SMA (myofibroblast marker) and VWF (endothelial cell marker). We observed increased co-localization (RVF: 5.0±0.1; Ctrl: 11.6±2.3, $p=0.047$) and number of VWF and α-SMA positive major vessels in PAH RV sections (RVF: 71.6±4.4%; Ctrl: 53.7±2.2%, $p=0.013$) compared to control (Figure 8C, D).

To validate the association of CTGF (CCN2) with EMT and RV failure, we measured the RV expression of CTGF protein in human PAH RV tissue using immunofluorescence. Similarly, we observed an increased expression of CTGF (CCN2) that localized primarily to

perivascular areas in human PAH RV tissue compared to control (RVF: 101.9±5.9; Ctrl: 82.8± 0.6 MFI per vessel, p=0.047) (Figure 8E, F).

Discussion

The present study is the first to conduct comparative RNA-seq analysis of RV between MCT- and SuHx-induced PAH animal models. We showed that MCT and SuHx rats shared similar gene expression profiles in RV. Furthermore, Hallmark and Reactome enrichment pathway analysis showed a significant shift in EMT, inflammation, and extracellular matrix organization, which is consistent with previous findings of RV failure from MCT- and SuHx-induced PAH models.[15,16] Also, this study revealed significant impairment of pathways related to metabolism such as oxidative phosphorylation, fatty acid metabolism, and respiratory electron transport. We provide translational relevance of our rat RV transcriptome using RV tissue from PAH patients to show evidence of EMT/EndMT and protein expression of a top EMT gene CCN2 (CTGF).

PAH animal models of RV failure

Traditionally, MCT rat model has been used to study RV failure, but off-target effects of MCT have greatly limited its translational relevance.[8,18] For example, myocarditis induced by MCT can affect both the left and right ventricle, which may complicate transcriptome results of RV hypertrophy and failure.[19] A recent transcriptomic study showed the gene expression profile of RV failure using MCT rat model, and compared it with published microarray data from pulmonary arterial banding (PAB) mice model and patients with bone morphogenetic protein receptor type 2 mutations (BRMP2).[20] Potus et al. showed significant metabolic changes involving mitochondria and electron transport chain, as well as fibrosis, inflammation, and angiogenesis.[20] Our MCT-RV expression profile is also in agreement with their results and previous reported studies. However, we include for the first time, the expression profile of RV from SuHx animal model using RNA sequencing, which is considered a more relevant pre-clinical model due to its pulmonary neointimal lesions that closely resemble human plexiform lesions.[9,21]

PAB model has been used alternatively to single injection of endothelial toxins to study RV remodeling since it is better tolerated and does not induce systemic or toxic effects. PAB is considered a pure RV pressure overload model without any pulmonary vascular injury. It typically results in far less RV decompensation and RV failure compared to MCT and SuHx animal models, and thus considered a better representation of RV adaptive remodeling.[2] A recent study comparing RV function of PAB with SuHx model showed that chronic progressive RV pressure overload alone does not cause RV failure, while RV failure from angioproliferative PAH results in exaggerated RVH, apoptosis, fibrosis, and capillary rarefaction.[22] Clinically, RV function from adult patients with PAH can still deteriorate despite significant reduction in PVR[23], and survival has been shown to be significantly associated with changes in RV ejection fraction as opposed to PVR or CO.[24] Based on these observations, we find MCT and SuHx to be appropriate models for understanding the molecular fingerprints of maladaptive RVH as opposed to adaptive RVH. In this study, we defined maladaptive RVH and RV failure from MCT and SuHx rats by significant elevation

of RVSP, decrease in PAT and PAT/PET ratio, RV dilation and fibrosis, which were confirmed prior to RNA sequencing. Thus, our results provide a comprehensive overview of genes involved in maladaptive RVH, but identifying key molecular determinants in the transition from adaptive to maladaptive RV remodeling are still needed.

Identification of top up-regulated genes in RV failure

Based on our differential expression analysis, the top up-regulated genes in the RV were SPP1 (Osteopontin, OPN) and AHRR (Aryl-Hydrocarbon Receptor Repressor) from MCT and SuHx rats, respectively. Previous reports have shown OPN, a matricellular cardiac fetal gene that is reactivated during cardiac stress, to be elevated in RV of MCT-induced RV failure rats, which can be reversed by estrogen.[14,25] OPN deletion has been shown to attenuate collagen deposition and deteriorate systolic function in the heart of angiotensin II-induced cardiac hypertrophy mouse model.[26] Also, RV remodeling and failure has been associated with extensive fibrosis, which is tightly linked to transformation growth factor beta (TGF-β) signaling, and changes in expression of extracellular matrix proteins and metalloproteinases.[27] We found that immunostaining of OPN in human RV tissue of patients with RV failure secondary to PAH localizes to interstitial and perivascular fibrotic areas (data not shown). Thus, these observations suggest a potential role of OPN in PAH-induced RV fibrosis.

Previous studies indicated that AHRR regulates AHR (aryl-hydrocarbon receptor), a basic helix-loop-helix transcription factor that acts as a receptor for endogenous metabolites and xenobiotics such as cigarette smoking.[28] AHRR mRNA is highly expressed in heart and brain[29], and plays a role in monocyte-to-macrophage differentiation[30], suppression of anti-inflammatory mediators[31], and tumor biology.[32] The role of AHRR in PAH and RV failure is unclear. Interestingly, studies have shown AHR and TGF-β signaling pathways to cross-regulate each other in a cell type-specific manner.[33,34] Given the role of TGF-β signaling in RV fibrosis, AHRR elevation may be involved in RV maladaptive remodeling in the setting of PAH.

EMT/EndMT activation in RV failure secondary to PAH

Based on our Hallmark enrichment analysis of RV from MCT and SuHx models, we identified up-regulated genes that were highly enriched in functions associated with EMT. EMT and EndMT play an integral role in early cardiovascular development, and are reactivated in numerous chronic cardiovascular disease states.[6,35] EMT/EndMT have been well characterized in myocardial fibrosis and diastolic dysfunction in pressure-overload rodent models[7,36], and play a critical role in tissue fibrosis and pulmonary vascular remodeling in PAH.[37] Given the evidence of EndMT in lungs of PAH patients[37] and cardiac fibrosis, and evidence of EndMT in RV of SuHx and MCT rats (Figure 6), we hypothesized that EndMT is most likely involved in RV failure of PAH patients. In this study, we identified five patients who met hemodynamic criteria for right-sided heart failure and either WHO group 1 (n=4) or group 3 (n=1) PH classification. MCT and SuHx models are considered more reflective of maladaptive RV hypertrophy in patients with WHO group 1 PAH.[2] We observed activation of EndMT by immunofluorescence using myofibroblast (α-SMA) and endothelial (VWF) markers. Further analysis of genes associated with EMT

based on Hallmark gene set showed SPP1 and CCN2 as the common top up-regulated genes in RV failure from MCT and SuHx rats. CCN2, also known as connective tissue growth factor (CTGF), is a matricellular protein that is induced in the heart following cardiac injury[38,39], and has been associated with the development of tissue fibrosis.[40] We observed increased CTGF immunolabeling and protein expression in RV of SuHx and MCT rats (Figure 7). In human RV sections, we observed an increased expression of CTGF in perivascular areas. Our results are in agreement with a recent study showing up-regulation of CTGF in PAH-mediated RV failure samples compared to non-failing RV by immunoblot.[41] Our findings using human RV tissue further validate the RV transcriptome from MCT and SuHx models, and highlight the importance of EMT/EndMT in RV failure secondary to PAH.

The role of inflammation in RV failure secondary to PAH

In our data, pro-inflammatory pathways were amongst some of the most up-regulated pathways in both models. Pro-inflammatory cytokines such as TNF-α, IL-1, and IL-6 have been associated with the development and progression of RV failure in PAH animal models.[15, 42–45] In MCT rats and PAB mice, expression of TNF-α in RV was increased[46] and contributed to adverse ventricular remodeling and dysfunction.[47] Decompensated RV failure from MCT model was also associated with increased TNF-α serum levels compared to compensated RV hypertrophy, suggesting a role of TNF-α as a biomarker for RV disease progression.[42,48] In addition, activation of NFkB has been associated with the development of cardiac hypertrophy and transition to heart failure.[49,50] A recent study showed an up-regulation of NFkB in RV of MCT model, which was modulated by exercise.[44] Attenuation of cardiovascular hemodynamics and RV hypertrophy in MCT-induced PAH by TNF-α antagonist suggests NFkB to be an important molecular mediator of TNF-α signaling.[51]

The role of metabolism in RV failure from PAH

We also identified multiple down-regulated genes in RV of MCT and SuHx rats that were involved with metabolism and fatty acid oxidation (FAO). During the process of RV adaptation and remodeling, there is a notable glycolytic shift in the RV of humans with PAH[52] and animal models of PAH.[53] For instance, RV hypertrophy from MCT- and PAB-induced PAH causes an increase in glycolysis and Glut1 expression, and pyruvate dehydrogenase kinase (PDK)-mediated inhibition of pyruvate dehydrogenase (PDH).[53] This PDK-mediated metabolic switch is associated with impaired RV contractility and decreased cardiac output, and electrical remodeling.[53,54]

FAO involvement in metabolic remodeling in RV failure remains unclear. A reciprocal relationship between FAO and glucose oxidation has been described (Randle's Cycle) in RVH, where inhibiting FAO and thereby increasing glucose oxidation can limit cellular damage.[55,56] In fact, recent studies using FAO inhibitors, trimetazidine and ranolazine, showed improvement of RV function by increasing glucose oxidation in PAB[55] and MCT models.[57] Another study in MCT-induced PAH rats showed impaired mitochondrial function and ADP channeling within the RV, and decreased ratio of mitochondria per myofibrillar proteins[58], which supports the role of energy metabolism in contributing to contractile dysfunction in the RV.[59]

Limitations

In this study, our RV transcriptomic signature represents maladaptive RV remodeling from hemodynamic pressure overload induced by MCT and SuHx. However, we cannot exclude the possibility that the direct toxic effects of MCT and SU5416 may have on the RV expression profile. Although both animal models induce PAH by different mechanisms, we identified significant overlap of DEGs and enriched pathways in the RV of MCT and SuHx rats. Given the similar expression profiles between MCT and SuHx rats, the development of RV failure was most likely initiated by the hemodynamic overload as opposed to direct systemic effects from endothelial toxins.

We also observed mild variability in expression profiles from animals exposed to SuHx as opposed to MCT. Previous reports showed hemodynamic variations in response to SuHx in different strains of rats or between colonies of the same strain.[60] A study using a similar protocol as our present study showed maximum RVSP and RV hypertrophy at 5-weeks and 3-weeks post-SU5416 injection in rats, respectively, followed by regression during normoxia exposure.[61] In this study, the exposure to normoxia prior to isolation of RV at 5-weeks post-injection may have attributed to the observed variability in RV hemodynamics and expression profiles between rats.

We acknowledge that our human RV tissue section from patients with PAH is a heterogenous group. It is plausible that patient's comorbidities such as systemic scleroderma may have contributed to the variability in histological staining. In addition, availability of normal RV sections was limited, and we observed prominent age-related cardiac fibrosis in one control patient. Direct comparison of expression profiles between MCT/SuHx and human would be ideal. Unfortunately, human RV tissue for RNA sequencing and public genomics data was not available to us.

Conclusions

Our RV transcriptomic signature of RV failure in MCT and SuHx animal models showed similar patterns of gene expression changes and biological pathways. Despite the inherent differences in PAH induction by MCT and SuHx models, the underlying pathways involved in RV maladaptation in response to pressure-load are similar. Histological confirmation of EndMT pathway and up-regulation of CTGF (CCN2) protein in human PAH-induced RV failure patients provide further validation of our RV transcriptomic findings. Targeting specific molecular mechanisms responsible for RV failure in both MCT and SuHx animal models may identify novel therapeutic strategies for PAH-associated RV failure.

Supplementary Material

Refer to Web version on PubMed Central for supplementary material.

Sources of funding:

NIH NHLBI Grant 1K08HL141995-01A1 (SU)

Non-standard Abbreviations and Acronyms

PAH	Pulmonary arterial hypertension
RV	Right ventricle
PVR	Pulmonary vascular resistance
EMT	Epithelial-to-mesenchymal transition
EndMT	Endothelial-to-mesenchymal transition
MCT	Monocrotaline
SuHx	Sugen hypoxia
RVSP	Right ventricular systolic pressure
PBS	Phosphate buffered saline
FDR	False discovery rate
PAT	Pulmonary artery acceleration time
RVIDd	RV internal diameter at end-diastole
FAO	Fatty acid oxidation
CTGF	Connective tissue growth factor

References

1. Zelt JGE, Chaudhary KR, Cadete VJ, Mielniczuk LM, Stewart DJ. Medical Therapy for Heart Failure Associated With Pulmonary Hypertension. Circ Res. 2019;124:1551–1567. [PubMed: 31120820]
2. Lahm T, Douglas IS, Archer SL, Bogaard HJ, Chesler NC, Haddad F, Hemnes AR, Kawut SM, Kline JA, Kolb TM, et al., American Thoracic Society Assembly on Pulmonary Circulation. Assessment of Right Ventricular Function in the Research Setting: Knowledge Gaps and Pathways Forward. An Official American Thoracic Society Research Statement. Am J Respir Crit Care Med. 2018;198:e15–e43. [PubMed: 30109950]
3. Rabinovitch M Molecular pathogenesis of pulmonary arterial hypertension. J Clin Invest. 2012;122:4306–4313. [PubMed: 23202738]
4. Rain S, Andersen S, Najafi A, Gammelgaard Schultz J, da Silva Gonçalves Bós D, Handoko ML, Bogaard H-J, Vonk-Noordegraaf A, Andersen A, van der Velden J, et al. Right Ventricular Myocardial Stiffness in Experimental Pulmonary Arterial Hypertension: Relative Contribution of Fibrosis and Myofibril Stiffness. Circ Heart Fail. 2016 7;9(7):e002636. [PubMed: 27370069]
5. Thiery JP, Acloque H, Huang RYJ, Nieto MA. Epithelial-mesenchymal transitions in development and disease. Cell. 2009;139:871–890. [PubMed: 19945376]
6. Kovacic JC, Mercader N, Torres M, Boehm M, Fuster V. Epithelial- and Endothelial- to Mesenchymal Transition: from Cardiovascular Development to Disease. Circulation. 2012;125:1795–1808. [PubMed: 22492947]
7. Zeisberg EM, Tarnavski O, Zeisberg M, Dorfman AL, McMullen JR, Gustafsson E, Chandraker A, Yuan X, Pu WT, Roberts AB, et al. Endothelial-to-mesenchymal transition contributes to cardiac fibrosis. Nat Med. 2007;13:952–961. [PubMed: 17660828]

8. Maarman G, Lecour S, Butrous G, Thienemann F, Sliwa K. A comprehensive review: the evolution of animal models in pulmonary hypertension research; are we there yet? Pulm Circ. 2013;3:739–756. [PubMed: 25006392]
9. Abe K, Toba M, Alzoubi A, Ito M, Fagan KA, Cool CD, Voelkel NF, McMurtry IF, Oka M. Formation of plexiform lesions in experimental severe pulmonary arterial hypertension. Circulation. 2010;121:2747–2754. [PubMed: 20547927]
10. Korotkevich G, Sukhov V, Sergushichev A. Fast gene set enrichment analysis. bioRxiv. 10 22, 2019. doi: 10.1101/060012
11. Liberzon A, Birger C, Thorvaldsdóttir H, Ghandi M, Mesirov JP, Tamayo P. The Molecular Signatures Database (MSigDB) hallmark gene set collection. Cell Syst. 2015;1:417–425. [PubMed: 26771021]
12. Jassal B, Matthews L, Viteri G, Gong C, Lorente P, Fabregat A, Sidiropoulos K, Cook J, Gillespie M, Haw R, et al. The reactome pathway knowledgebase. Nucleic Acids Res. 2020;48:D498–D503. [PubMed: 31691815]
13. Subramanian A, Tamayo P, Mootha VK, Mukherjee S, Ebert BL, Gillette MA, Paulovich A, Pomeroy SL, Golub TR, Lander ES, et al. Gene set enrichment analysis: a knowledge-based approach for interpreting genome-wide expression profiles. Proc Natl Acad Sci USA. 2005;102:15545–15550. [PubMed: 16199517]
14. Nadadur RD, Umar S, Wong G, Eghbali M, Iorga A, Matori H, Partow-Navid R, Eghbali M. Reverse right ventricular structural and extracellular matrix remodeling by estrogen in severe pulmonary hypertension. J Appl Physiol (1985). 2012;113:149–158. [PubMed: 22628376]
15. Sydykov A, Mamazhakypov A, Petrovic A, Kosanovic D, Sarybaev AS, Weissmann N, Ghofrani HA, Schermuly RT. Inflammatory Mediators Drive Adverse Right Ventricular Remodeling and Dysfunction and Serve as Potential Biomarkers. Front Physiol. 2018; 9: 609. [PubMed: 29875701]
16. Ryan JJ, Archer SL. The Right Ventricle in Pulmonary Arterial Hypertension: Disorders of metabolism, angiogenesis and adrenergic signaling in right ventricular failure. Circ Res. 2014;115:176–188. [PubMed: 24951766]
17. Li Y, Lui KO, Zhou B. Reassessing endothelial-to-mesenchymal transition in cardiovascular diseases. Nat Rev Cardiol. 2018;15:445–456. [PubMed: 29748594]
18. Gomez-Arroyo JG, Farkas L, Alhussaini AA, Farkas D, Kraskauskas D, Voelkel NF, Bogaard HJ. The monocrotaline model of pulmonary hypertension in perspective. Am J Physiol Lung Cell Mol Physiol. 2012;302:L363–369. [PubMed: 21964406]
19. Miyauchi T, Yorikane R, Sakai S, Sakurai T, Okada M, Nishikibe M, Yano M, Yamaguchi I, Sugishita Y, Goto K. Contribution of endogenous endothelin-1 to the progression of cardiopulmonary alterations in rats with monocrotaline-induced pulmonary hypertension. Circ Res. 1993;73:887–897. [PubMed: 8403258]
20. Potus F, Hindmarch CCT, Dunham-Snary KJ, Stafford J, Archer SL. Transcriptomic Signature of Right Ventricular Failure in Experimental Pulmonary Arterial Hypertension: Deep Sequencing Demonstrates Mitochondrial, Fibrotic, Inflammatory and Angiogenic Abnormalities. Int J Mol Sci. 2018; 12;19(9):2730.
21. Taraseviciene-Stewart L, Kasahara Y, Alger L, Hirth P, Mc Mahon G, Waltenberger J, Voelkel NF, Tuder RM. Inhibition of the VEGF receptor 2 combined with chronic hypoxia causes cell death-dependent pulmonary endothelial cell proliferation and severe pulmonary hypertension. FASEB J. 2001;15:427–438. [PubMed: 11156958]
22. Bogaard Harm J, Natarajan Ramesh, Henderson Scott C, Long Carlin S, Kraskauskas Donatas, Smithson Lisa, Ockaili Ramzi, McCord Joe M, Voelkel Norbert F Chronic Pulmonary Artery Pressure Elevation Is Insufficient to Explain Right Heart Failure. Circulation. 2009;120:1951–1960. [PubMed: 19884466]
23. Veerdonk MC van de, Kind T, Marcus JT, Mauritz G-J, Heymans MW, Bogaard H-J, Boonstra A, Marques KMJ, Westerhof N, Vonk-Noordegraaf A Progressive Right Ventricular Dysfunction in Patients With Pulmonary Arterial Hypertension Responding to Therapy. J Am Coll Cardiol. 2011;58:2511–2519. [PubMed: 22133851]

24. Girgis RE. Predicting Long-Term Survival in Pulmonary Arterial Hypertension: More Than Just Pulmonary Vascular Resistance. Journal of the American College of Cardiology. 2011;58:2520–2521. [PubMed: 22133852]
25. Imoto K, Okada M, Yamawaki H. Expression profile of matricellular proteins in hypertrophied right ventricle of monocrotaline-induced pulmonary hypertensive rats. J Vet Med Sci. 2017;79:1096–1102. [PubMed: 28496027]
26. Matsui Y, Jia N, Okamoto H, Kon S, Onozuka H, Akino M, Liu L, Morimoto J, Rittling SR, Denhardt D, Kitabatake A, Uede T. Role of osteopontin in cardiac fibrosis and remodeling in angiotensin II-induced cardiac hypertrophy. Hypertension. 2004;43:1195–1201. [PubMed: 15123578]
27. Bogaard HJ, Abe K, Vonk Noordegraaf A, Voelkel NF. The Right Ventricle Under Pressure: Cellular and Molecular Mechanisms of Right-Heart Failure in Pulmonary Hypertension. Chest. 2009;135:794–804. [PubMed: 19265089]
28. Mimura J, Ema M, Sogawa K, Fujii-Kuriyama Y. Identification of a novel mechanism of regulation of Ah (dioxin) receptor function. Genes Dev. 1999;13:20–25. [PubMed: 9887096]
29. Bernshausen T, Jux B, Esser C, Abel J, Fritsche E. Tissue distribution and function of the Aryl hydrocarbon receptor repressor (AhRR) in C57BL/6 and Aryl hydrocarbon receptor deficient mice. Arch Toxicol. 2006;80:206–211. [PubMed: 16205913]
30. Saeed S, Quintin J, Kerstens HHD, Rao NA, Aghajanirefah A, Matarese F, Cheng S-C, Ratter J, Berentsen K, van der Ent MA, et al. Epigenetic programming of monocyte-to-macrophage differentiation and trained innate immunity. Science. 2014;345:1251086. [PubMed: 25258085]
31. Awji EG, Chand H, Bruse S, Smith KR, Colby JK, Mebratu Y, Levy BD, Tesfaigzi Y. Wood smoke enhances cigarette smoke-induced inflammation by inducing the aryl hydrocarbon receptor repressor in airway epithelial cells. Am J Respir Cell Mol Biol. 2015;52:377–386. [PubMed: 25137396]
32. Opitz CA, Litzenburger UM, Sahm F, Ott M, Tritschler I, Trump S, Schumacher T, Jestaedt L, Schrenk D, Weller M, et al. An endogenous tumour-promoting ligand of the human aryl hydrocarbon receptor. Nature. 2011;478:197–203. [PubMed: 21976023]
33. Chang X, Fan Y, Karyala S, Schwemberger S, Tomlinson CR, Sartor MA, Puga A. Ligand-Independent Regulation of Transforming Growth Factor β1 Expression and Cell Cycle Progression by the Aryl Hydrocarbon Receptor. Molecular and Cellular Biology. 2007;27:6127–6139. [PubMed: 17606626]
34. Wolff S, Harper PA, Wong JMY, Mostert V, Wang Y, Abel J. Cell-Specific Regulation of Human Aryl Hydrocarbon Receptor Expression by Transforming Growth Factor-β1. Mol Pharmacol. 2001;59:716–724. [PubMed: 11259615]
35. Lamouille S, Xu J, Derynck R. Molecular mechanisms of epithelial–mesenchymal transition. Nature Reviews Molecular Cell Biology. 2014;15:178–196. [PubMed: 24556840]
36. Kovacic JC, Mercader N, Torres M, Boehm M, Fuster V. Epithelial- and Endothelial- to Mesenchymal Transition: from Cardiovascular Development to Disease. Circulation. 2012;125:1795–1808. [PubMed: 22492947]
37. Ranchoux B, Antigny F, Rucker-Martin C, Hautefort A, Péchoux C, Bogaard H-J, Dorfmüller P, Remy S, Lecerf F, Planté S, et al. Endothelial-to-Mesenchymal Transition in Pulmonary Hypertension. Circulation. 2015;131:1006–1018. [PubMed: 25593290]
38. Chen MM, Lam A, Abraham JA, Schreiner GF, Joly AH. CTGF Expression is Induced by TGF- β in Cardiac Fibroblasts and Cardiac Myocytes: a Potential Role in Heart Fibrosis. Journal of Molecular and Cellular Cardiology. 2000;32:1805–1819. [PubMed: 11013125]
39. Ahmed MS, Øie E, Vinge LE, Yndestad A, Øystein Andersen G, Andersson Y, Attramadal T, Attramadal H. Connective tissue growth factor--a novel mediator of angiotensin II-stimulated cardiac fibroblast activation in heart failure in rats. J Mol Cell Cardiol. 2004;36:393–404. [PubMed: 15010278]
40. Leask A, Abraham DJ. All in the CCN family: essential matricellular signaling modulators emerge from the bunker. J Cell Sci. 2006;119:4803–4810. [PubMed: 17130294]

41. Williams JL, Cavus O, Loccoh EC, Adelman S, Daugherty JC, Smith SA, Canan B, Janssen PML, Koenig S, Kline CF, et al. Defining the molecular signatures of human right heart failure. Life Sciences. 2018;196:118–126. [PubMed: 29366750]
42. Campian ME, Hardziyenka M, de Bruin K, van Eck-Smit BLF, de Bakker JMT, Verberne HJ, Tan HL. Early inflammatory response during the development of right ventricular heart failure in a rat model. Eur J Heart Fail. 2010;12:653–658. [PubMed: 20495202]
43. Ahmed LA, Obaid AAZ, Zaki HF, Agha AM. Role of oxidative stress, inflammation, nitric oxide and transforming growth factor-beta in the protective effect of diosgenin in monocrotaline-induced pulmonary hypertension in rats. European Journal of Pharmacology. 2014;740:379–387. [PubMed: 25062790]
44. Nogueira-Ferreira R, Moreira-Gonçalves D, Silva AF, Duarte JA, Leite-Moreira A, Ferreira R, Henriques-Coelho T. Exercise preconditioning prevents MCT-induced right ventricle remodeling through the regulation of TNF superfamily cytokines. Int J Cardiol. 2016;203:858–866. [PubMed: 26599752]
45. Wang J-J, Zuo X-R, Xu J, Zhou J-Y, Kong H, Zeng X-N, Xie W-P, Cao Q. Evaluation and Treatment of Endoplasmic Reticulum (ER) Stress in Right Ventricular Dysfunction during Monocrotaline-Induced Rat Pulmonary Arterial Hypertension. Cardiovasc Drugs Ther. 2016;30:587–598. [PubMed: 27844183]
46. Luitel H, Sydykov A, Schymura Y, Mamazhakypov A, Janssen W, Pradhan K, Wietelmann A, Kosanovic D, Dahal BK, Weissmann N, et al. Pressure overload leads to an increased accumulation and activity of mast cells in the right ventricle. Physiol Rep. 2017; 5(6): e13146. [PubMed: 28330950]
47. Sun M, Chen M, Dawood F, Zurawska U, Li JY, Parker T, Kassiri Z, Kirshenbaum LA, Arnold M, Khokha R, Liu PP. Tumor necrosis factor-alpha mediates cardiac remodeling and ventricular dysfunction after pressure overload state. Circulation. 2007;115:1398–1407. [PubMed: 17353445]
48. Paulin R, Sutendra G, Gurtu V, Dromparis P, Haromy A, Provencher S, Bonnet S, Michelakis ED. A miR-208-Mef2 axis drives the decompensation of right ventricular function in pulmonary hypertension. Circ Res. 2015;116:56–69. [PubMed: 25287062]
49. Gupta S, Young D, Maitra RK, Gupta A, Popovic ZB, Young SL, Mahajan A, Wang Q, Sen S. Prevention of Cardiac Hypertrophy and Heart Failure by Silencing of NF-κB. J Mol Biol. 2008;375:637–649. [PubMed: 18037434]
50. Maier HJ, Schips TG, Wietelmann A, Krüger M, Brunner C, Sauter M, Klingel K, Böttger T, Braun T, Wirth T. Cardiomyocyte-specific IκB kinase (IKK)/NF-κB activation induces reversible inflammatory cardiomyopathy and heart failure. Proc Natl Acad Sci USA. 2012;109:11794–11799. [PubMed: 22753500]
51. Wang Q, Zuo X, Wang Y, Xie W, Wang H, Zhang M. Monocrotaline-induced pulmonary arterial hypertension is attenuated by TNF-α antagonists via the suppression of TNF-α expression and NF-κB pathway in rats. Vascular Pharmacology. 2013;58:71–77. [PubMed: 22846229]
52. Rich S, Pogoriler J, Husain AN, Toth PT, Gomberg-Maitland M, Archer SL. Long-term Effects of Epoprostenol on the Pulmonary Vasculature in Idiopathic Pulmonary Arterial Hypertension. Chest. 2010;138:1234–1239. [PubMed: 21051399]
53. Piao L, Fang Y-H, Cadete VJJ, Wietholt C, Urboniene D, Toth PT, Marsboom G, Zhang HJ, Haber I, Rehman J, Lopaschuk GD, Archer SL. The inhibition of pyruvate dehydrogenase kinase improves impaired cardiac function and electrical remodeling in two models of right ventricular hypertrophy: resuscitating the hibernating right ventricle. J Mol Med. 2010;88:47–60. [PubMed: 19949938]
54. Archer SL, Fang Y-H, Ryan JJ, Piao L. Metabolism and bioenergetics in the right ventricle and pulmonary vasculature in pulmonary hypertension. Pulm Circ. 2013;3:144–152. [PubMed: 23662191]
55. Fang Y-H, Piao L, Hong Z, Toth PT, Marsboom G, Bache-Wiig P, Rehman J, Archer SL. Therapeutic inhibition of fatty acid oxidation in right ventricular hypertrophy: exploiting Randle's cycle. J Mol Med. 2012;90:31–43. [PubMed: 21874543]
56. Zhang R, Jing ZC. Energetic Metabolic Roles in Pulmonary Arterial Hypertension and Right Ventricular Remodeling. Current Pharmaceutical Design. 2016;22(31):4780–4795. [PubMed: 27306090]

57. Rocchetti M, Sala L, Rizzetto R, Staszewsky LI, Alemanni M, Zambelli V, Russo I, Barile L, Cornaghi L, Altomare C, et al. Ranolazine prevents INaL enhancement and blunts myocardial remodelling in a model of pulmonary hypertension. Cardiovasc Res. 2014;104:37–48. [PubMed: 25139747]

58. Gomez-Arroyo J, Mizuno S, Szczepanek K, Van Tassell B, Natarajan R, dos Remedios Cristobal G., Drake JI., Farkas L, Kraskauskas D, Wijesinghe DS, et al. Metabolic Gene Remodeling and Mitochondrial Dysfunction in Failing Right Ventricular Hypertrophy Secondary to Pulmonary Arterial Hypertension. Circulation: Heart Failure. 2013;6:136–144. [PubMed: 23152488]

59. Power AS, Norman R, Jones TLM, Hickey AJ, Ward M-L. Mitochondrial function remains impaired in the hypertrophied right ventricle of pulmonary hypertensive rats following short duration metoprolol treatment. PLoS One. 2019 9;14(4):e0214740. [PubMed: 30964911]

60. Jiang B, Deng Y, Suen C, Taha M, Chaudhary KR, Courtman DW, Stewart DJ. Marked Strain-Specific Differences in the SU5416 Rat Model of Severe Pulmonary Arterial Hypertension. Am J Respir Cell Mol Biol. 2016;54:461–468. [PubMed: 26291195]

61. Toba M, Alzoubi A, O'Neill KD, Gairhe S, Matsumoto Y, Oshima K, Abe K, Oka M, McMurtry IF. Temporal hemodynamic and histological progression in Sugen5416/hypoxia/normoxia-exposed pulmonary arterial hypertensive rats. Am J Physiol Heart Circ Physiol. 2014;306:H243–H250. [PubMed: 24240870]

Clinical Perspective

What is new?

- The present study is the first to conduct comparative transcriptomic analysis of RV between MCT- and SuHx-induced PH animal models.
- The validation of EMT/EndMT as the top common pathway in both pre-clinical rat models of severe PH and the evidence of EMT/EndMT in human RV failure are novel findings of this study.

What are the clinical implications?

- PH-induced RV failure is a significant prognostic determinant of morbidity and mortality.
- The mechanistic details of RV failure, especially the regulatory control of the key pathways still remain unclear.
- The transcriptomic signature of RV failure in MCT and SuHx rat models showed similar patterns of gene expression changes and biological pathways in this study.
- Confirmation of EndMT pathway and up-regulation of CTGF (CCN2) protein in RV failure patients provide further validation of our RV transcriptomic findings.
- Targeting specific molecular mechanisms responsible for RV failure in MCT and SuHx models may identify novel therapeutic strategies for PAH-associated RV failure in humans.

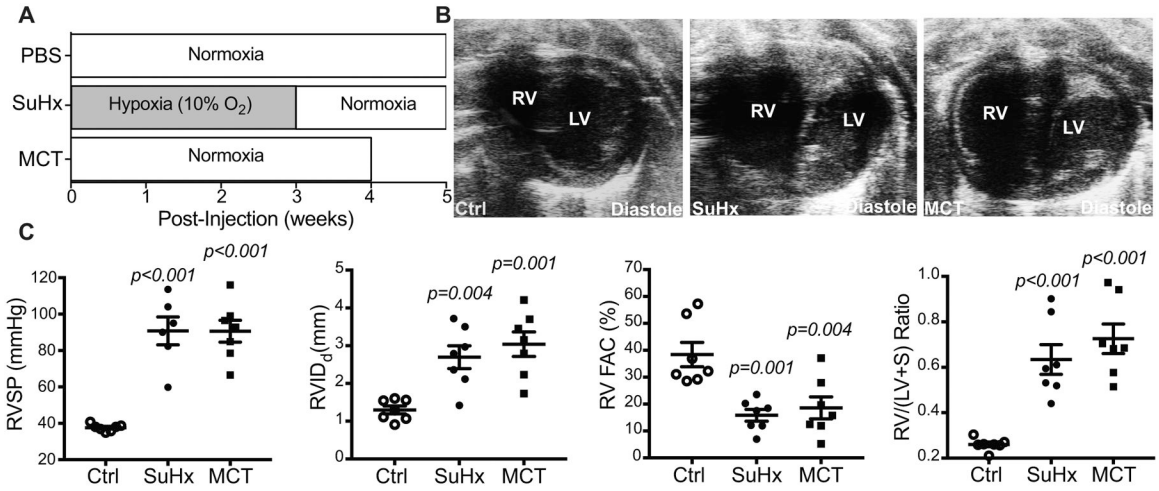

Figure 1.

Development of RV failure in PAH rats. (A) Experimental protocol for MCT, SuHx, and PBS (Ctrl) treated rats. (B) Representative echocardiographic images of RVFAC from parasternal short-axis views at end-diastole. (C) Terminal hemodynamic assessment of RVSP, summary of echocardiographic assessment of RV function ($RVID_d$, RVFAC), and RV hypertrophy Fulton index (RV weight/LV weight + IVS weight). Data presented as mean ± SD. N= 6–7 rats per group.

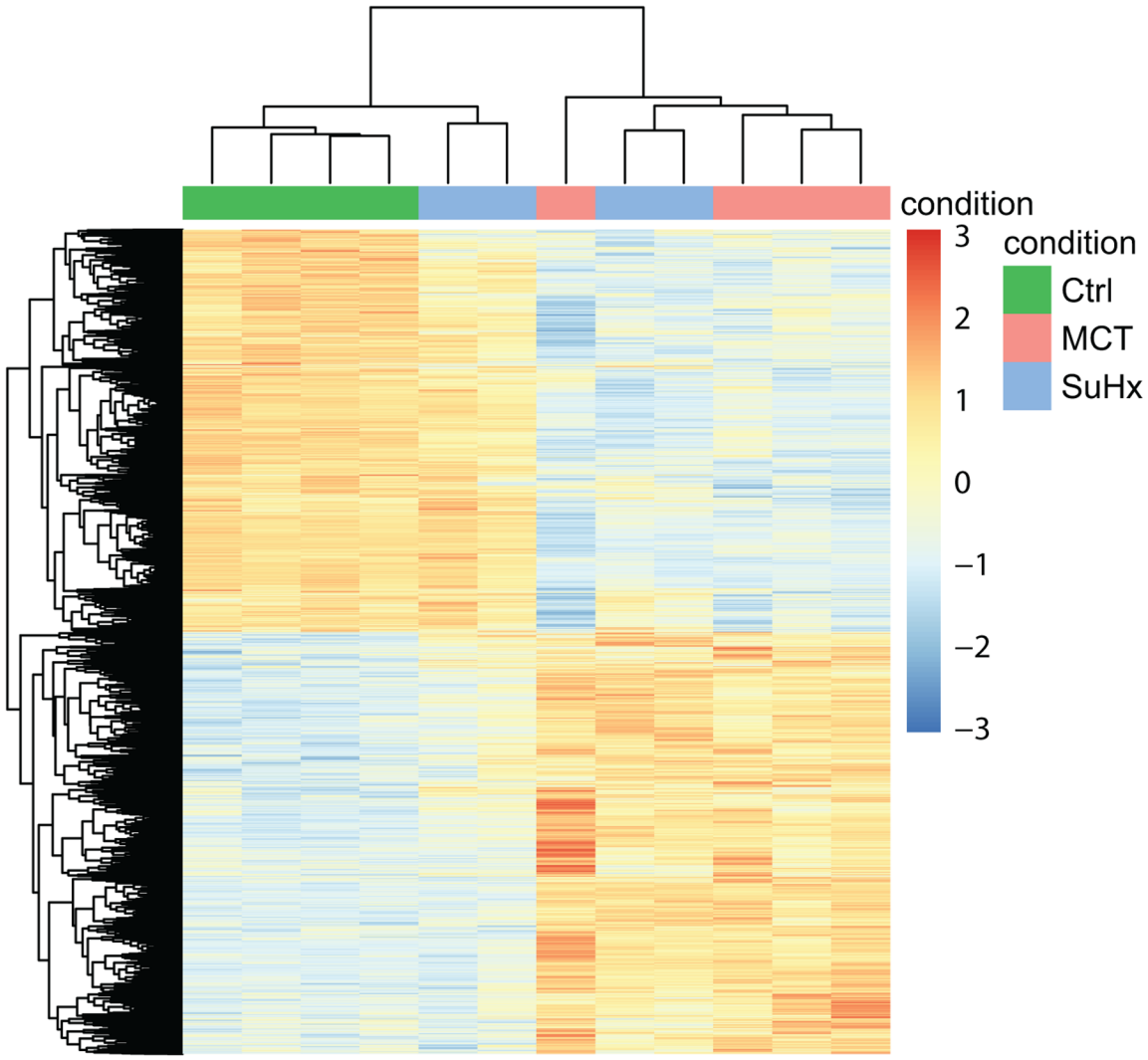

Figure 2.

Heat map showing top differentially expressed genes in RV with FDR<0.05 of SuHx (blue) compared to MCT (red) and control (Ctrl; green) group. Gene expression scaled by row. N=4 rats per group.

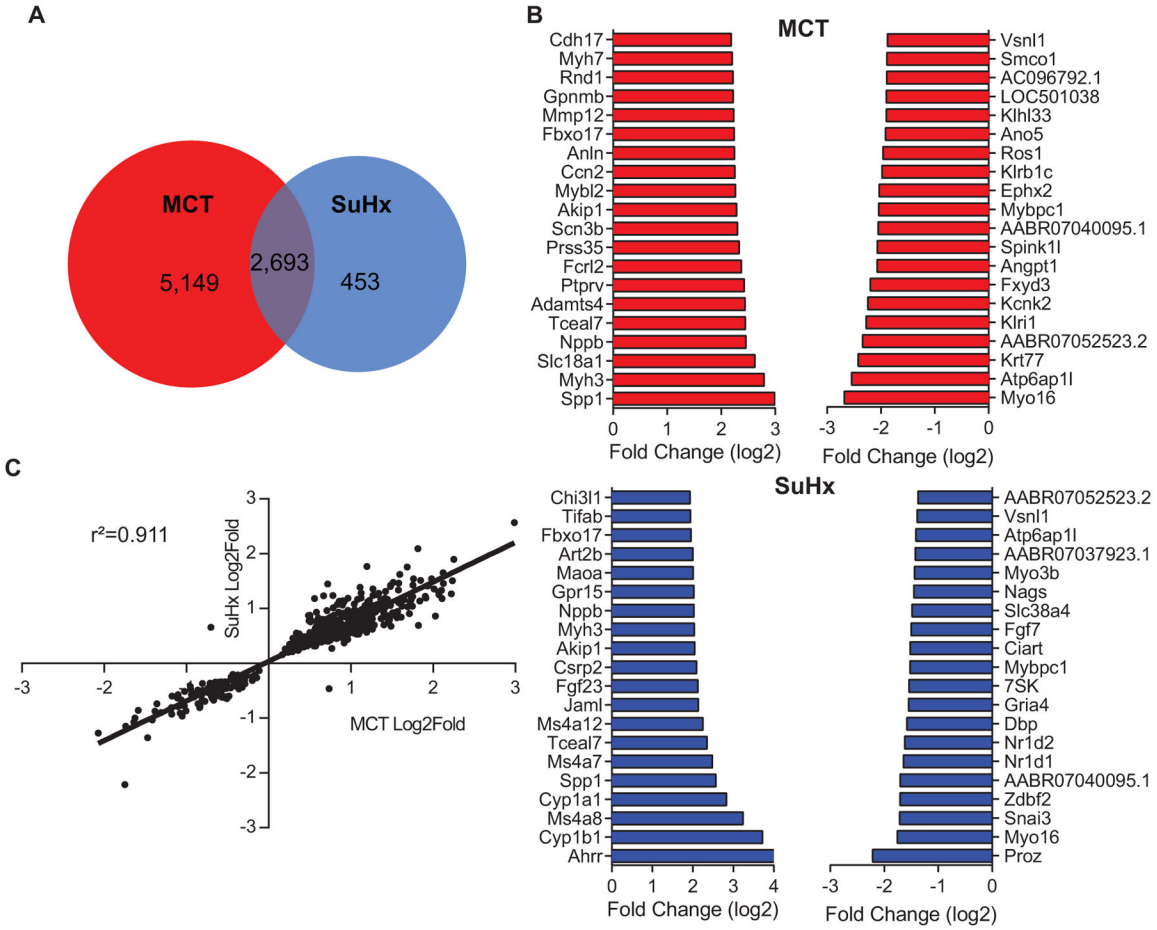

Figure 3.

Common and unique DEGs in RV of MCT and SuHx rats. (A) Venn diagram representing total overlapping DEGs of MCT and SuHx rats that were considered statistically significant according to FDR <0.05 compared to control. (B) The top 20 up-regulated (*left*) and down-regulated (*right*) DEGs from MCT (*red, top*) and SuHx (*blue, bottom*) rats based on log2fold and FDR <0.05 compared to control. (C) Scatter plot of overlapping DEGs between MCT and SuHx with an R-squared of 0.911. N=4 per group.

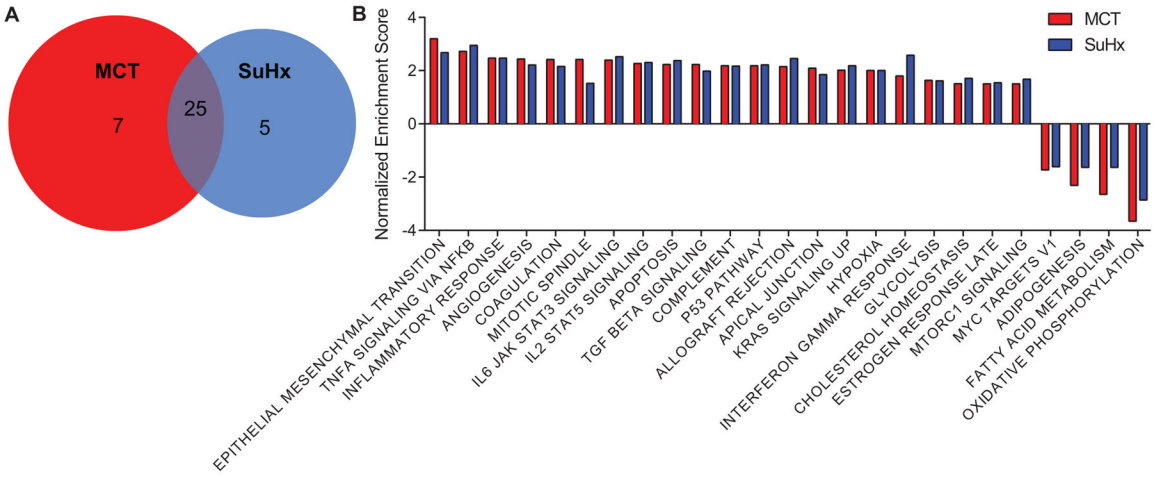

Figure 4.

Hallmark pathways analysis of DEGs in RV of MCT and SuHx rats. (A) Venn diagram showing total number and overlapping pathways of MCT (red) vs SuHx (blue) with false discovery rate <0.05 compared to control. (B) Hallmark pathway enrichment analysis of overlapping pathways of MCT and SuHx rats. N=4 per group.

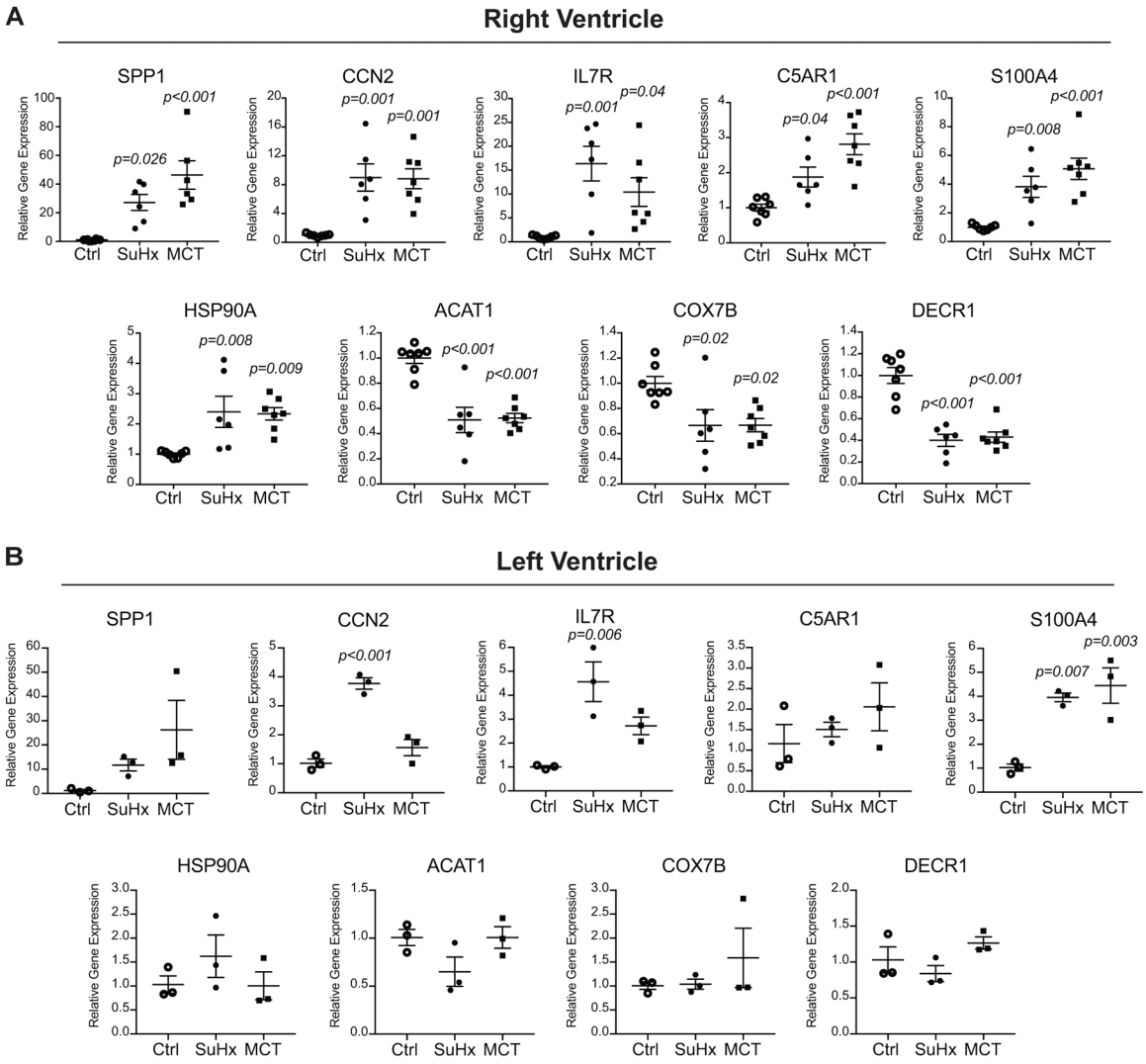

Figure 5.

qPCR validation of DEGs in RV (A) and LV (B) of Ctrl, SuHx, and MCT rats. Mean ± SD, n=6–7 per group for RV and n=3 per group for LV.

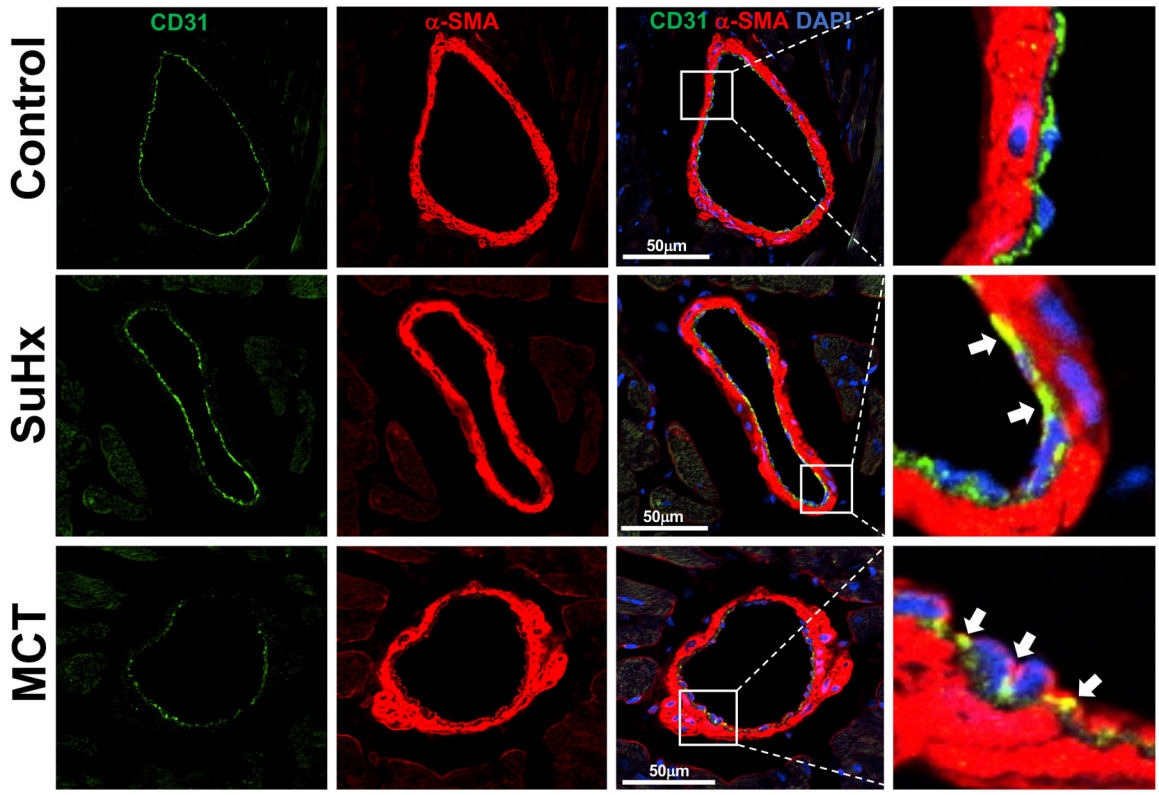

Figure 6.

Rat PH-mediated RV failure is associated with increased EndMT in RV. Representative images of immunofluorescence staining with antibodies against α-SMA (red) and CD31 (green) in rat RV sections from Control, SuHx and MCT groups. Arrows indicate vessels positive for both α-SMA and CD31. Arrowheads indicate co-localization (yellow). N=3 rats per group.

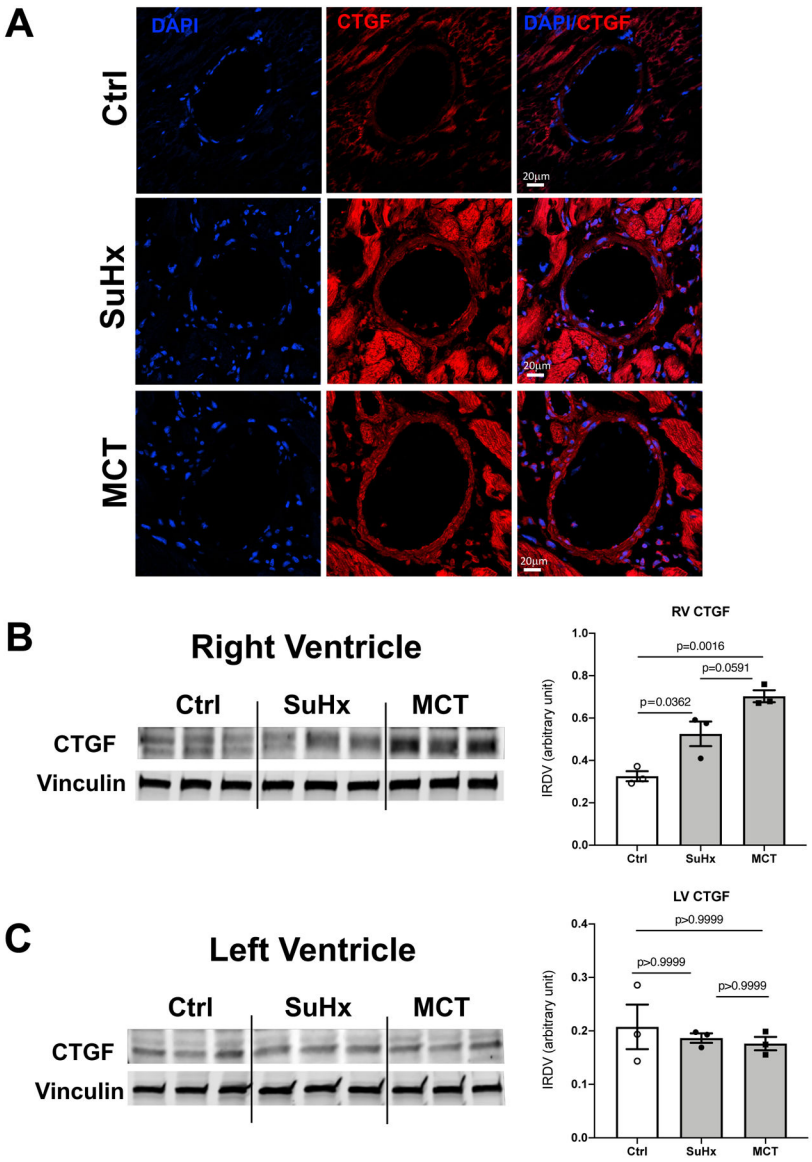

Figure 7.

Rat PH-mediated RV failure is associated with increased CTGF (CCN2) expression in RV. (A) Representative images of immunofluorescence staining with antibody against CCN2 (CTGF, red) in RV sections from Control, SuHx and MCT rats. Nuclei stained with 4′,6-diamidino-2-phenylindole (DAPI) in blue. (B, C) Quantification of CTGF (~38 KD) expression in RV and LV tissue of Control, SuHx and MCT rats. Vinculin (~117 KD) was used as a control. Mean ± SD, n=3 per group.

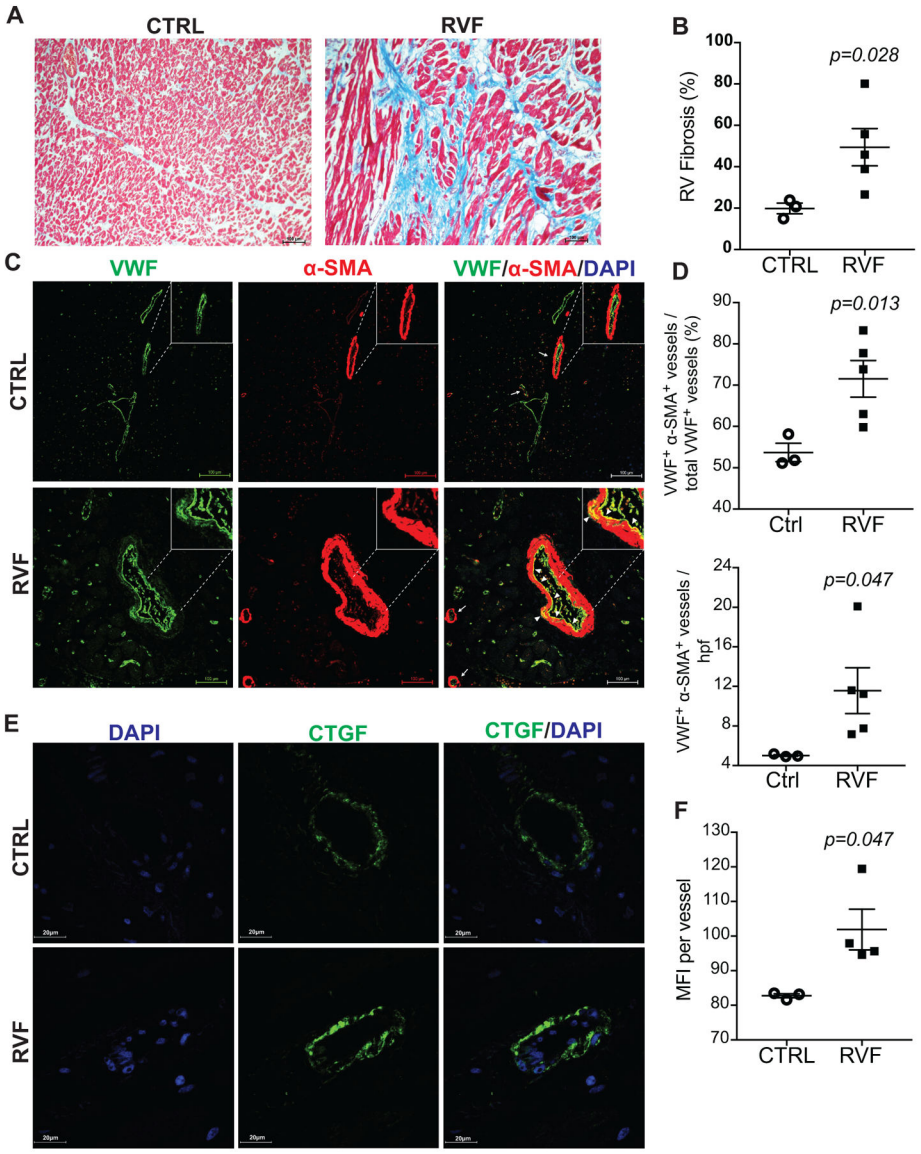

Figure 8.

Human PAH-mediated RV failure is associated with increased fibrosis, EndMT, and expression of CCN2 (CTGF). (A) Trichome staining of human RV cross-sections from PAH-mediated RV failure (RVF) and non-heart failure (CTRL) patients. Red and blue represents cardiomyocytes and collagen deposition (fibrosis), respectively. (B) Quantification of %RV fibrosis in RVF (n=5) and CTRL (n=3) patients. (C) Representative images of immunofluorescence staining with antibodies against α-SMA (red) and VWF (green) in human RV sections. Arrows indicate vessels positive for both α-SMA and VWF. Arrowhead indicates co-localization (yellow). (D) Quantification of major vessels positive for both α-SMA and VWF in RVF (n=5) and CTRL (n=3) patients by percentage of total VWF^+ vessels and counts per high power field (hpf). (E) Representative images of immunofluorescence staining with antibody against CCN2 (CTGF, green) in RV sections from RVF and CTRL patients. Nuclei stained with 4′,6-diamidino-2-phenylindole (DAPI) in

blue. (F) Quantification of CTGF expression in RV sections from RVF (n=5) and CTRL (n=3) patients by mean fluorescence intensity (MFI) per major vessel. Mean ± SD. Unpaired t-test.

Table 1.

Echocardiography evaluation of SuHx and MCT rats.

	Control (n=7)	SuHx (n=7)	MCT (n=7)
RVFAC (%)	38.4 ± 12.0	15.8 ± 5.7**	18.6 ± 10.8**
PAT (ms)	29.4 ± 4.2	18.5 ± 2.3***	21.1 ± 6.2**
PAT/PET	0.4 ± 0.0	0.2 ± 0.0***	0.3 ± 0.1***
$RVID_d$ (mm)	1.3 ± 0.3	2.7 ± 0.8**	3.0 ± 0.9***
LVEF (%)	81.7 ± 9.8	91.2 ± 9.0	81.6 ± 11.8
LVFS (%)	53.1 ± 9.5	68.6 ± 16.3	57.7 ± 17.7
HR (bpm)	346 ± 40	376 ± 117	302 ± 36
RVSP (mmHg)	37.6 ± 2.0	90.8 ± 18.7***	90.6 ± 16.0***
RV/(LV+S)	0.3 ± 0.0	0.6 ± 0.2***	0.7 ± 0.2***

Mean ± SD. N= 6–7 rats per group.

* p<0.05;

** p<0.01;

*** p<0.001.

RVFAC: right ventricle fractional area change; PAT: pulmonary artery acceleration time; PET: pulmonary ejection time; RVIDd: right ventricle internal diameter at end-diastole; LVEF: left ventricular ejection fraction; LVFS: left ventricular fractional shortening; HR: heart rate; RVSP: right ventricular systolic pressure; RV: right ventricle, LV: left ventricle; S: septum.